This is a repository copy of *Aqueous-based assembly of plant-derived proteins yields a crosslinker-free biodegradable bioplastic consistent with green chemistry principles*.

Aqueous-Based Assembly of Plant-Derived Proteins Yields a Crosslinker-Free Biodegradable Bioplastic Consistent with Green Chemistry Principles

Amit Kumar Sarkar,*[a, b] Ziyu Yang,[a] Tal Astruc,[a] and Nadav Amdursky*[a, c]

Plastics are an indispensable part of modern life. Due to the harmful environmental consequences of petroleum-based plastic usage, there is an urgent need to replace them with biodegradable bioplastics that meet the sustainability standards required for a low environmental footprint. Here, we use plant-derived proteins to produce bioplastics. Since most plant-derived proteins are not water-soluble, there has always been a need to use acidic or basic solutions or organic solvents with plasticizers and crosslinkers to produce bioplastic. Here, we present a counterintuitive approach for using water-insoluble plant-derived soy and pea proteins to manufacture large-scale bioplastics using only water as a solvent without common plasticizers or crosslinkers. We show that bioplastics can form via a self-assembly process initiated by a small molecular initiator while maintaining favourable mechanical properties. The lack of crosslinking and the protein nature of the bioplastic leads to a rapid biodegradation process under various conditions. Overall, the approach we present is highly attractive in terms of cost and time, and most importantly, it obeys all the relevant principles of green chemistry in bioplastics production.

Introduction

Plastics developed from fossil-fuel-derived polymers have significant detrimental environmental consequences. They lead to the emission of dangerous greenhouse gases and the accumulation of persistent plastic waste, eventually inhibiting our society's carbon-neutral economic development.[1–3] Consequently, in light of environmental regulatory measures, a substantial effort is being made to develop 'environmentally friendly plastic' that meets sustainability standards. Such standards obey green chemistry principles, such as atom economy, prevention, safe chemicals/solvents, design for energy efficiency, and design for degradation.[4–6] Many approaches for producing environmentally friendly plastics, commonly called bioplastics, use bio-based building blocks. These approaches can be roughly divided into synthetic approaches, i.e., chemical polymerization of low molecular weight monomers or exploiting bio-derived polymeric biomacromolecules (polysaccharides

or proteins) from raw biomass, as well as biotechnological approaches involving genetic engineering for the production of mainly proteins.[7–10] It is important to note that while the end-of-life aspects of bioplastics, i.e., their biodegradability, are often considered superior, many bioplastics are slowly to non-biodegradable, depending on the synthetic approach, such as chemical polymerizations[11] or crosslinking reactions.[12] Moreover, many bioplastics are not produced using green chemistry methodologies nor helping in lowering the carbon footprint of plastic. To date, bioplastics constitute less than 2% of the plastics used, partly due to their production cost and performance.[13]

This work focuses on the use of biomacromolecules for manufacturing bioplastics. The state-of-the-art of this class uses mainly carbohydrates[14–16] and proteins,[17–23] which can be extracted from waste sources of various industries. From an environmental and carbon footprint point of view, plant-derived proteins are considered a renewable resource, and they have a negative carbon footprint,[24] hence their use is superior to animal-derived proteins. To date, practically all plant-derived proteins that can be extracted in mass quantities from raw biomass have been used in bioplastics production.[18,25–33] Here, we use soy protein (SoyP) and pea protein (PeaP). The standard method for producing bioplastics from plant-derived proteins is via solution processing using single or mixed solvent-based strategies, such as organic solvents,[30,34] acids,[12,29] bases,[12,35–40] additives[36,41,42]/plasticizers,[12,35,36,39,41,42] or crosslinkers.[32,37,39,40,43] For instance, in one of the novel SoyP films produced by the Knowles group,[29] they used 30% acetic acid as solvent and heated the solution to 90°C together with ultrasonication to solubilize the SoyP, subsequently adding the glycerol plasticizers in 20–40 wt% to produce the final bioplastic. Accordingly, developing a robust aqueous-based bioplastic formulation from plant-derived proteins with minimal processing stages and a

[a] Schulich Faculty of Chemistry, Technion–Israel Institute of Technology, Haifa, Israel
[b] College of Engineering and Physical Sciences, Aston University, Birmingham, United Kingdom
[c] Department of Chemistry, University of Sheffield, Sheffield, United Kingdom

Correspondence: Amit Kumar Sarkar and Nadav Amdursky, Schulich Faculty of Chemistry, Technion–Israel Institute of Technology, Haifa 3200003, Israel.
Email: a.sarkarpol@gmail.com and amdursky@technion.ac.il and n.amdursky@sheffield.ac.uk

suitable balance between mechanical stability to on-demand degradation and biodegradation is the 'holy grail' to unlock the sustainability potential for utilizing plant-derived proteins for bioplastics.

Here, we introduce an aqueous-based counterintuitive green chemistry approach for making bioplastic sheets using food-grade plant-derived proteins. Both SoyP and PeaP are not water soluble at the concentrations required for bioplastic processing. As mentioned, to date, processing of SoyP and PeaP for bioplastics involved the dissolution of the proteins in various solutions, mostly containing acids or bases, followed by the introduction of plasticizers and crosslinkers. Our methodology is counterintuitive since we start with the nonsoluble state of the protein in water, i.e., a cloudy solution containing protein aggregates. At this stage, we add a small quantity of an initiating molecule, a small alpha hydroxy acid, glycolic acid (GlyA),[44–46] that is present in most plants and is used in various production processes. Upon water evaporation, GlyA initiates the protein's self-assembly process for producing the bioplastic with attractive mechanical properties without adding any common plasticizer or crosslinker. We show that the water evaporation-assisted self-assembly process is accompanied by a change in the protein secondary structure. Our new bioplastics can be degraded in water on demand, a property that can be tuned by a simple chemical process, thus allowing the recyclability of the bioplastic within minutes to hours, which opens new possibilities for upcycling the bioplastic. Most importantly, due to the processing methodology, our bioplastics are rapidly biodegradable in soil and aqueous environments in several days. As most of our bioplastic is composed solely of food-grade proteins, its disposal and subsequent bio/degradation can be beneficial for the environment and used as a fertilizer. Overall, this straightforward water-based processing of commercial plant-derived proteins into bioplastics with attractive properties can be highly promising for numerous applications.

Results and Discussion

Processing Strategy

The new process we introduce here (schematically presented in Figure 1a) starts by suspending either SoyP or PeaP powder (at 7 wt%) in pure water. As stated, both SoyP and PeaP are water-insoluble; thus, they create a light brown dispersion in an aqueous environment. At this stage, the protein dispersion is slightly heated (to 50 °C), followed by the addition of GlyA (at a final 0.25 0.2 wt%), resulting in a milky dispersion. Then, the milky dispersion is cast into a plastic container (using plastic is essential, as will be discussed below). Following water evaporation, a transparent film is formed (Figure 1b and Figure S1. In general, all results presented in the main text are for SoyP films; the PeaP films, which share the same processing methodology, are detailed in the Supporting Information). The final water content of the dry film was calculated to be 4.7 ± 0.5 wt%. The film formation requires a minimum processing temperature of 50 °C, as films were not formed at room temperature, whereas >50 °C similar films with similar properties were formed. Due to energy considerations, we recommend the use of 50 °C. The
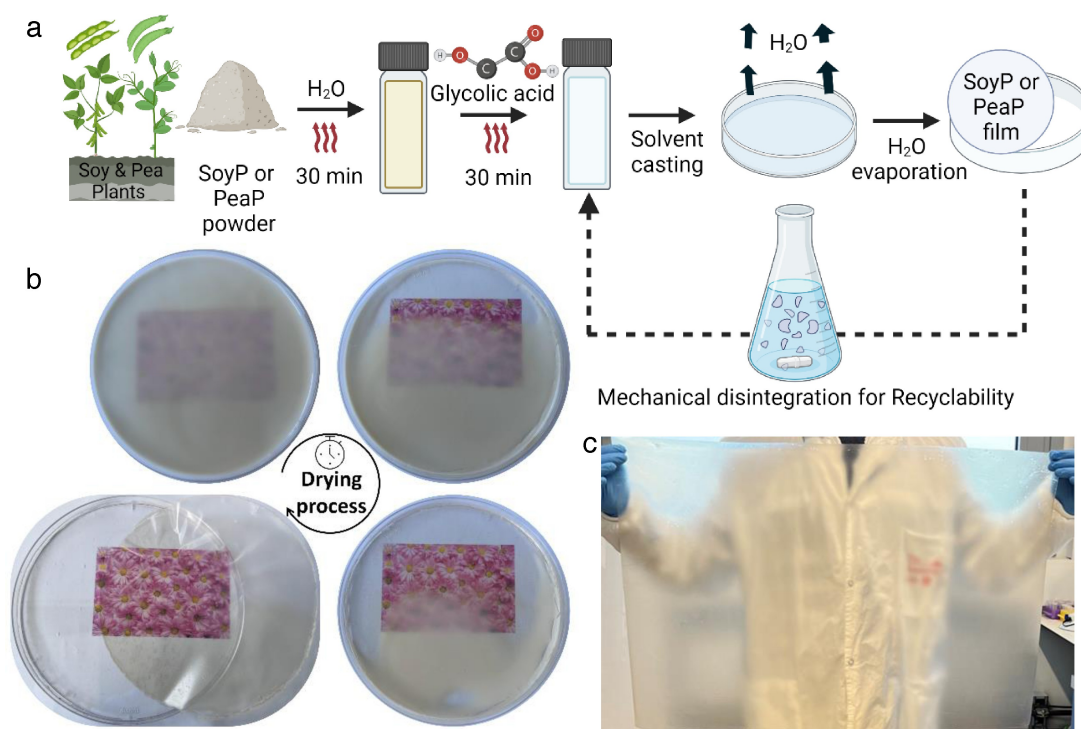

Figure 1. Processing strategy. a, Schematic diagram of the processing strategy of plant-derived protein films. b, The gradual evolution of a SoyP film with time (clockwise, starting at the top left). c, Image of a large-scale SoyP film (50×70 cm).

entire process is demonstrated in the detailed scheme, highlighting its simplicity. Since all materials used in the process, i.e., SoyP/PeaP, GlyA (in very small amounts), and water are highly available and affordable, process scale-up to large film sheets is straightforward (Figure 1c).

 

Structural Characterization

The first question that arises is: *what is the mechanism of the observed process?* Firstly, the use of GlyA in the process does not resemble the use of plasticizers since GlyA addition results in protein agglomeration (as indicated by the color change of the dispersion) and the quantities used for GlyA are lower than the conventional use of plasticizers. Moreover, no free-standing film is formed without the use of GlyA; hence, it is essential to the process. Notably, previous SoyP-based films required the use of plasticizers such as glycerol and crosslinkers or other linker materials, in either very basic or acidic reaction conditions.[47,48] The transformation from a brownish to white dispersion after adding GlyA and, finally, to a transparent film after water evaporation is indicative of an interaction between the proteins and GlyA. Moreover, as the slight heating before

adding GlyA is also important for film production, it also indicates a structural change in the protein. In the next sections, we will follow the changes in the protein structure during the self-assembly process into free-standing film formation, which will allow us to determine the mechanism.

Secondary Structure Analysis via FTIR

First, we used FTIR to gain insight into the changes in the protein's secondary structure during assembly, from dry powder through the aqueous environment to dry film formation (Figure 2a). In general, the FTIR spectrum of a protein is sensitive to the $>C=O$ stretching of amide I ($\sim$1600–1700 cm^{-1}), the bending of N–H, and the stretching of C–N of amide II ($\sim$1500–1600 cm^{-1}), which are all sensitive to the secondary structure of the protein.[49–51] Additionally, the $\sim$3100–3300 cm^{-1} region is linked to O–H absorption, associated mainly with the presence of water.

As shown in Figure 2a, a clear change in the FTIR spectra is observed from the dry SoyP powder to SoyP film via hydrated SoyP suspension and SoyP-GlyA suspension. The indicative amide II peak at 1530 cm^{-1} for dry SoyP powder became less prominent upon interaction with water at 50 °C. Next, the
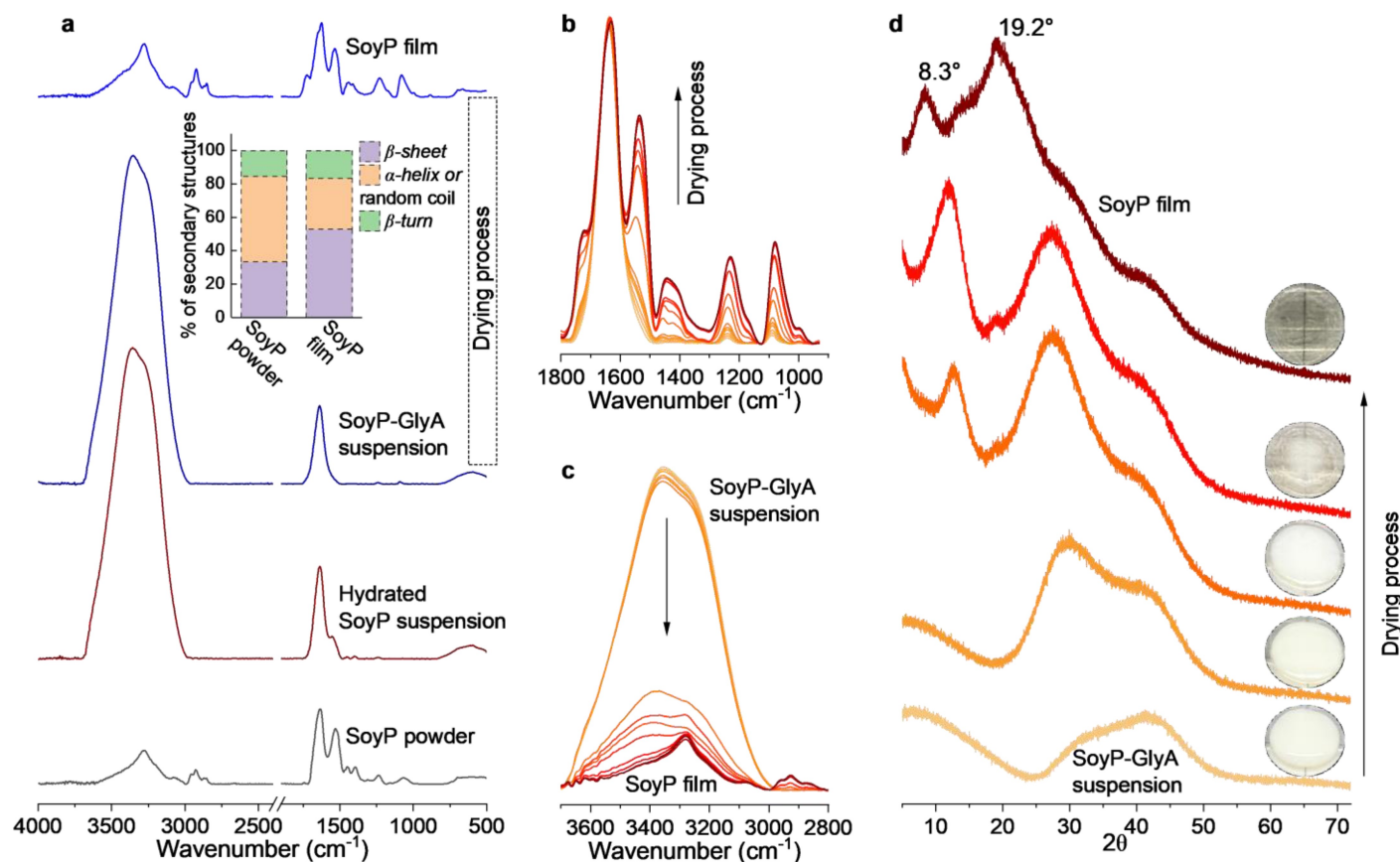
Figure 2. Structural characterization. a, FTIR spectra at different stages of the SoyP film production. The inset shows the extracted protein secondary structure, derived from the second derivative of the FTIR spectra in the amide I region for the SoyP powder and film. b, and c, Time-dependent in situ FTIR analysis of the drying process starting from the SoyP-GlyA suspension (orange curves) until film formation (dark red curves), focusing on the amide bonds area (panel b) and the water-associated O–H absorption region (panel c). d, Time-dependent in situ XRD analysis of the drying process starting from the SoyP-GlyA suspension (orange curves) until film formation (dark red curves). The insets show pictures of the sample at each stage during measurement.

ChemSusChem

Research Article
doi.org/10.1002/cssc.202401567

Chemistry
Europe
European Chemical
Societies Publishing

addition of GlyA leads to a complete elimination of this amide II peak. Interestingly, we noticed the regeneration of the amide II peak in the dry SoyP film with an additional hump at ~1725 cm^{-1}, whereas the latter can be ascribed to the incorporation of carboxylic groups from GlyA in the SoyP film (Figure S2 for the PeaP). The regeneration of the amide II peak at 1530 cm^{-1} is accompanied by the loss of water, as can be observed in the time-dependent in situ FTIR measurement during drying, from the protein-GlyA suspension until film formation (Figure 2b and c depict the amide II and water regions, respectively). The changes in the amide II position already indicate a change in the secondary structure during the process. It is also important to note that some of the other peaks, which are mostly associated with C−H vibrations, e.g., the stretching vibration at ~2800–2900 cm^{-1}, cannot be observed in the hydrated steps due to the masking by water molecules.

We further used the amide I region (1600–1700 cm^{-1}) to elucidate the protein's secondary structural contributions (Figure 2a, inset) using a second derivative and deconvoluting the outcome to the well-known characteristic protein conformations for *β-sheet*, *α-helix or random coils*, and *β-turns*.[50,51] Importantly, we compared only the spectra of the SoyP powder and the final SoyP film as it is not valid to compare dry and hydrated samples using this methodology. As observed in the inset of Figure 2a, the protein within the film configuration is adopting a more *β-sheet*-rich secondary structure compared to the starting SoyP powder material. Thus, indicating that the film formation process involves a structural change of the protein (as will be detailed below).

The Films' Crystallinity and Periodicity

While we can resolve the changes in the protein secondary structure during film formation from the FTIR measurements, we are still missing the last piece of the puzzle when the magic happens: *What process occurs during water evaporation that transforms the agglomerated protein to a transparent film?* To understand the mechanism of this last step and any periodicity during the generation of the protein film, we turned to real-time X-ray diffraction (XRD) measurements (Figure 2d). In this measurement, we followed the process starting from the GlyA-treated SoyP milky-white suspension until it became transparent (Figure 2d, insets). Immediately after drop-casting, the XRD pattern of the drop-cast GlyA-treated SoyP suspension shows a broad hump corresponding to the amorphous nature of the suspension. From this point, we can observe a time-dependent transformation of the XRD pattern. It begins with the emergence of a semipeak-like appearance at 2θ of ~29° that becomes narrower with time and shifts to lower 2θ values to a newly generated crystalline-like peak at 2θ of ~12°, which also shifts towards lower 2θ values at longer times. Finally, upon complete water evaporation, the film exhibits well-defined peaks with obtained 2θ values at 8.3° and 19.02°, corresponding to distances of 10.6 Å and 4.6 Å, respectively (Figure 2d and Figure S3 for the PeaP film).

The periodicity observed in the final film's XRD study is a result of the ordered secondary structure within the film, formed only upon water evaporation and the self-assembly process (as discussed in the FTIR section). The 10.6 Å and 4.6 Å peaks are well-defined characteristics of ordered *β-sheet* structures, as also observed in other SoyP-based materials or films using other methodologies.[52–55] Overall, the XRD measurements further indicate the self-assembly process by which the proteins change their structure and periodicity during water evaporation.

The Mechanism of Film Formation

In this section, we suggest the film formation mechanism (Figure 3). First, we summarize the necessary conditions and requirements for the process:

- Both SoyP and PeaP have a large percentage (>27%) of carboxylic acid-containing amino acids, aspartic (Asp) and glutamic (Glu) acids (Tables S1A–B and S2 A–B, Supplementary Information, for SoyP and PeaP, respectively). This is necessary for film production, as we found that other plant-based proteins with smaller percentages, such as the zein protein, could not be used in the presented methodology.
- Slight heating to 50 °C during the first steps is essential.
- The addition of GlyA, an alpha-hydroxy acid, is essential for the assembly process. We found that adding lactic acid (the second smallest alpha-hydroxy acid) can also result in film formation. However, adding small non-alpha-hydroxy acids, such as acetic acid or glycine, did not result in similar film formation.
- Finally, it is evident from the methodology that water molecules play a major role in the process, both before drop-casting and during the assembly process.

These requirements have led us to suggest the following steps in the process of the protein film production (Figure 3):

1 A powder of natively folded SoyP/PeaP proteins is the starting point of the process.

2 Placing the powder in pure water results in the deprotonation of Glu and Asp, thus producing carboxylates, resulting in repulsion between the protein chains. This process, together with the slight heating of the system, leads to changes in the protein structure. At this stage, a dispersion of the protein is formed. As shown by our FTIR measurements, we can already see a change in the protein secondary structure upon exposure to water.

3 Adding GlyA to the system results in the immediate agglomeration of the protein. Although GlyA is a weak acid, it lowers the pH of the water solution to below 4, resulting in the protonation of most carboxylic acids in the system. This is possible only when pure water is used, while using a buffer (i.e., preventing the drop in the pH upon adding GlyA) does not allow film formation. The carboxylic acid-containing residues (Glu/Asp) can form hydrogen bonds, resulting in protein aggregation. This stage is accompanied by an additional change in the protein structure as shown by the FTIR measurements. Since water molecules are present in the
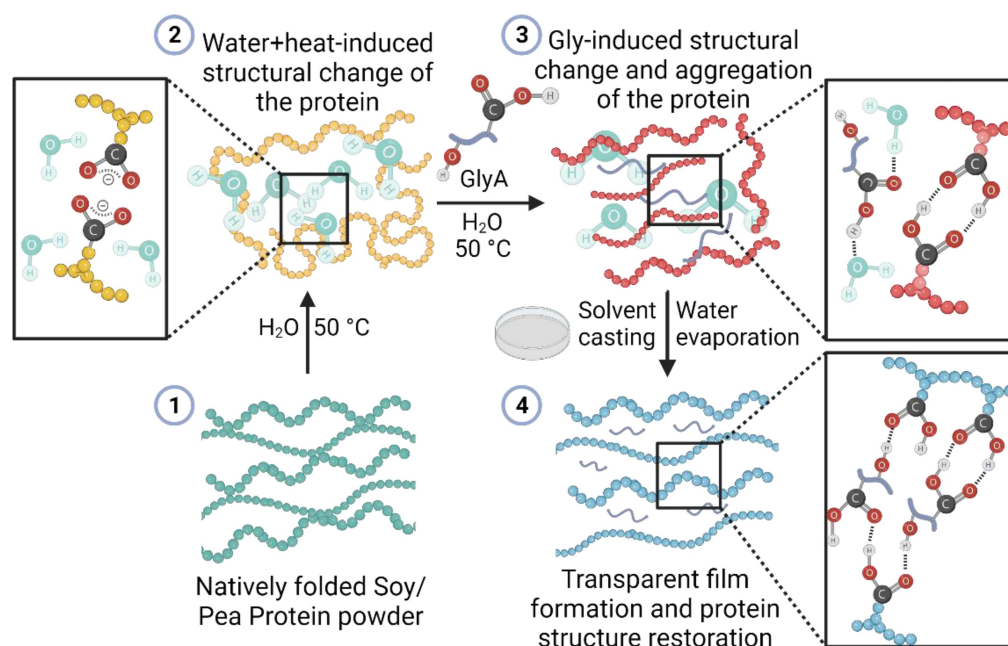
Figure 3. Mechanism of film formation. The suggested processes and the accompanying changes in protein structure (represented by a different color of the protein chain) occurring during protein film formation at the different stages: 1) before the process; 2) after forming the protein suspension in water; 3) after the addition of GlyA to the suspension; and 4) after water evaporation and film formation.

system, they can also form hydrogen bonds, both with the amino acids and with GlyA, thus 'shielding' from the integration of GlyA between the protein chains.

4 The last step is the water evaporation-assisted assembly process. When water molecules leave the system, the GlyA molecules can be incorporated between the protein chains. Since GlyA is an alpha-hydroxy acid, both its −OH and −COOH groups can assist in a hydrogen-bond network formation. This step is accompanied by a change in the protein secondary structure to a β-sheet-rich structure, as shown by FTIR, and the transition from an amorphous structure to an ordered semi-crystalline film, as shown by XRD. The end result is an ordered assembled film, prompting its transparency.

Since the assembly process for producing the transparent free-standing film is based on hydrogen bonding between the protein chains, it gives rise to two properties of the film. The first property is the film's ability to self-heal, which aligns with numerous other films and gels.[52,56,57] Accordingly, two pieces of the protein film can be healed together (Figure S4 and Movie S1). The second property is related to the material on which the film is formed. We have found that the film can be easily removed only when drop-casting is performed on a rather hydrophobic substrate, such as plastic or Teflon. On the other hand, when glass or silica is used as the substrate material, the formed film adheres strongly to the substrate and cannot be removed from it due to hydrogen bonds between the proteins/GlyA and the substrate.

Mechanical and Morphological Properties

The tensile testing of the protein film displays a nontraditional mechanical property (Figure 4a and Figure S5 for the PeaP film). Initially, a sharp increase in stress (up to ~4 MPa) can be observed at relatively small strain values, resulting in a tensile strength of ~7 MPa and a calculated Young's modulus of ~220 MPa (Table S3). However, after the initial increase in stress, a plateau in measured stress is observed up to strain values of ~110%. Finally, with increasing strain, we observe a second increment of stress until the film reaches its ultimate elongation at a fracture of ~250% (Table S3). This three-stage stress-strain curve pattern is uncommon in protein-based films; however, mechanical-induced transition in protein structure is well known for keratin proteins.[58] Accordingly, the observed three-stage pattern might be related to a structural transition within the film. To gain further insight into this transition, we followed the XRD pattern after stretching the film (Figure 4b and Figure S6 for the PeaP film). The XRD demonstrates a formation of highly crystalline peaks, i.e., increasing periodicity at the positions ascribed to the β-sheet structures within the films, only after stretching. We further followed the FTIR pattern of the SoyP film in the stretching area (Figure S7a) from the stretched region of the SoyP film, indicating no fundamental difference in the FTIR pattern. We observeed only a minor change in the extracted secondary structure components by calculating the protein secondary structure components from the FTIR spectra (Figure S7b). Thus, we can conclude that stretching induces an ordering of the structure within the film with no major indications of a change in the secondary structure.
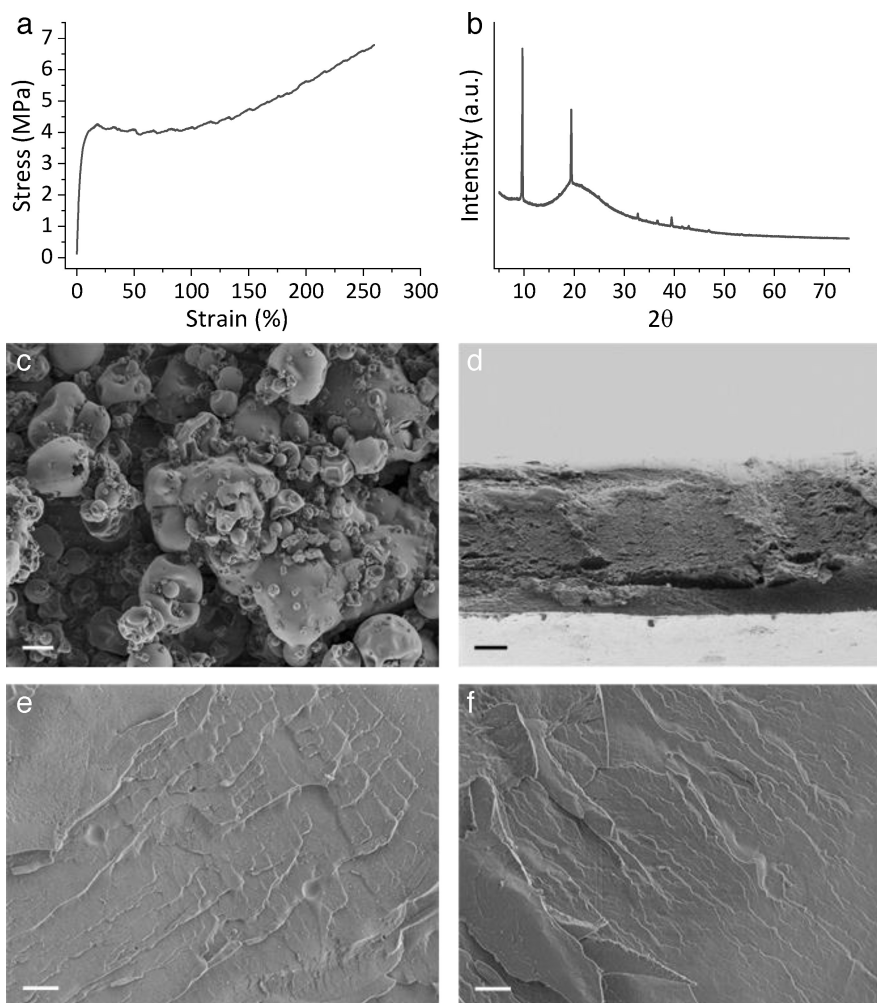
ChemSusChem

Research Article
doi.org/10.1002/cssc.202401567

Chemistry Europe
European Chemical
Societies Publishing

Figure 4. Mechanical and morphological properties. a, Tensile stress-strain testing of the SoyP film. b, XRD pattern of a strained SoyP film. SEM analysis of c, SoyP powder, and d, cross-sectioned SoyP film. Cryo-SEM analysis of e, SoyP suspension and f, SoyP-GlyA suspension. Scale bars in c and d represent 20 μm, and in e and f represent 2 μm.

To follow the morphology of the film microstructure, we turned to scanning electron microscopy (SEM). First, we compared the powder at the starting point and the final film configuration, showing that the microstructures of the two dry forms differed. While the powder has a granular structure (Figure 4c), the film comprises dense and interconnected thin layers (Figure 4d for the film cross-section). We further used cryo-SEM to evaluate whether the aggregates within the aqueous environment before and after adding GlyA contained any morphological/microstructural features. We found that both solutions contained aggregates with some noticeable layer microstructure but a featureless morphology (Figure 4e and f). The lack of noticeable morphology is in contrast to the study by Knowles and colleagues,[29] where they observed a clear fibrillar structure during their assembly process to produce a SoyP film, highlighting the different mechanisms for SoyP film production despite the same starting material.

Adjusting the Stability of the Protein Film

So far, we have introduced the process for manufacturing a free-standing film composed of dense and interconnected thin layers from an agglomerated protein solution via a hydrogen-bonding-driven self-assembly mechanism. The next immediate question is related to the stability of the film in various conditions, especially considering the film's starting material, SoyP/PeaP, and the unique self-assembly process that relies on hydrogen bonding in contrast to conventional covalent cross-linking. The stability of the film is of prime importance, considering the practical viability of our protein bioplastics as a replacement for fossil-fuel-derived plastics. We first explore the stability under ambient conditions (room temperature and humidity) by following the intactness of the protein film placed on a bench in our lab. No noticeable change in the film was found for over a year; it did not degrade and remained elastic, even under different environmental conditions, i.e., the relative humidity of the surroundings.

The second important stability assay was performed in water. Due to the involvement of hydrogen bonding in the self-assembly process, water can easily penetrate the film, resulting in rapid and large water uptake of ~150 wt% within 5 minutes in water and nearly 280 wt% after 120 minutes (Figure 5a). During water uptake, and again, due to the involvement of hydrogen bonding in the assembly process, water enters the film and interacts with both the protein side chains and the GlyA molecules, resulting in the film starting to collapse. At the end of this process, the film is dispersed into the form of the milky-white agglomerated dispersion. Whereas the films are stable in various humidity conditions, the water uptake into the film (up to ~100 wt%) considerably lowers the tensile strength of the materials (Figure S8), which are still intact but less strong due to the presence of water in them.

We further found that the dispersion of the film in water can be significantly accelerated using mechanical agitation, resulting in forming a dispersion within several minutes. Importantly, we established that the film can be easily recycled

in this manner. Consequently, we can reform the film by mechanically agitating the film in pure water solution until it is dispersed within a few minutes, followed by drop casting (as shown in Figure 1a).

As stated, the water uptake into the film will result in its eventual collapse and dispersion in water. While the dispersion of the film within several hours in an aqueous environment should not limit most of the practical applications of the bioplastic (primarily for packaging), it might be a limiting factor for aqueous-based applications. Accordingly, we discovered an easy and straightforward step to enhance the aqueous stability of the film by restricting water uptake. To restrict water uptake, the interconnected layer structure of the film must be made much denser. To this aim, we simply dipped the film in methanol (MeOH) for 10 min, known to strengthen the hydrogen bonding between proteins.[59] Upon MeOH dipping, we found that the film's microstructure had significantly changed, resulting in a much denser film configuration, and the interconnected thin layers are not visible anymore (Figure 5b).
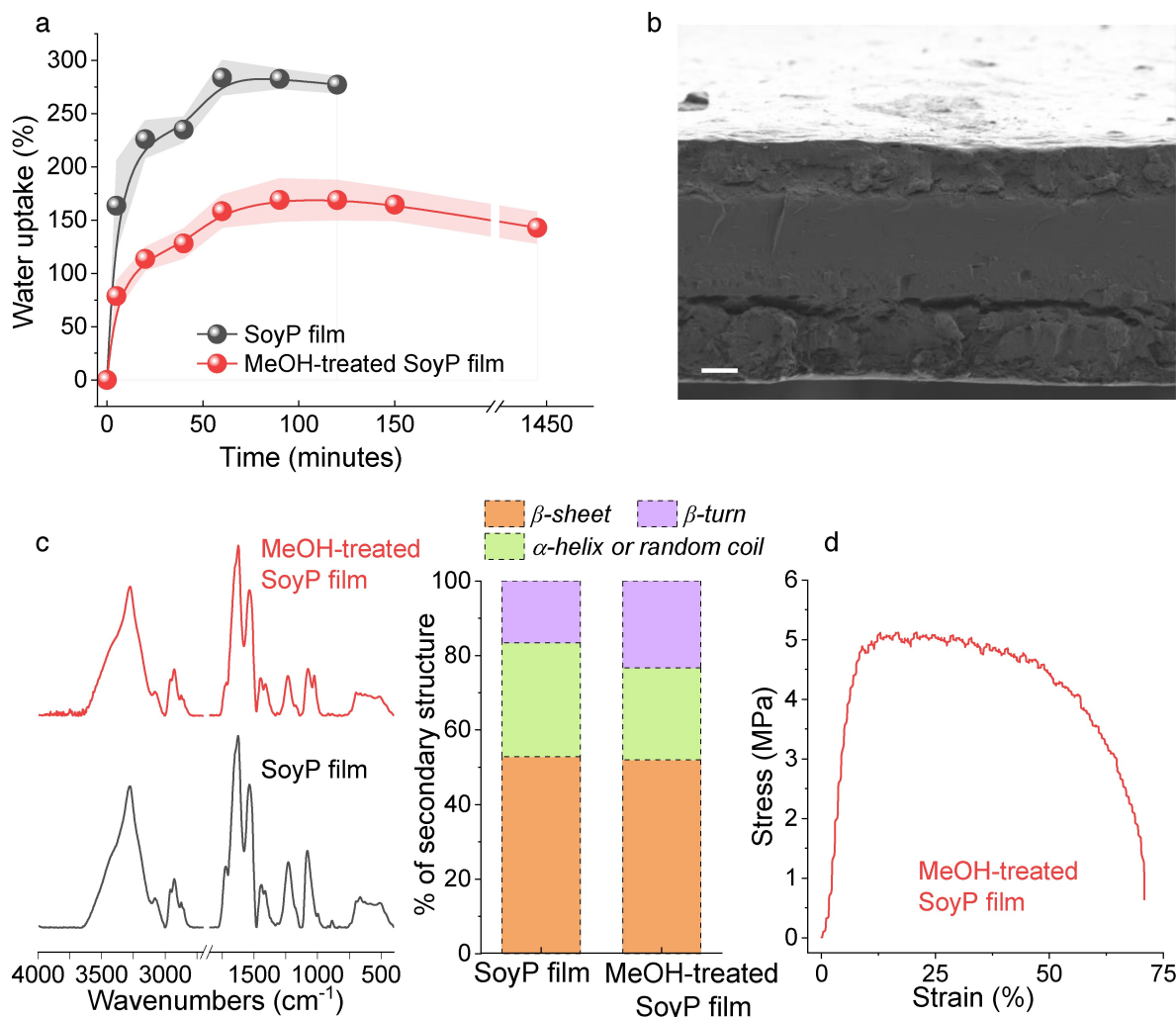
Figure 5. Tuning the stability of the protein film. a, Comparative analyses of water uptake as a function of time for the SoyP film before and after MeOH treatment. The shaded area represents the standard deviation of N = 3 samples. b, SEM image of the cross-section of a MeOH-treated SoyP film. The scale bar represents 20 μm. c, Comparative FTIR spectra of the SoyP film before and after MeOH treatment (left panel) together with the extracted percentage of secondary structure derived from the second derivative of the FTIR spectra (right panel). d, Tensile stress-strain testing of the MeOH-treated SoyP film.

ChemSusChem

Research Article
doi.org/10.1002/cssc.202401567

Chemistry
Europe
European Chemical
Societies Publishing

Importantly, we found that the water uptake of the MeOH-treated film is considerably lower than before the MeOH treatment and that the film maintained its structural integrity for ~2 days within an aqueous environment (Figure 5a). In terms of protein structure, we compared the FTIR spectrum of the film before and after MeOH dipping, which revealed a generally similar pattern with relatively similar extracted secondary structure components (Figure 5c). The dense micro-structure of the MeOH-treated film is responsible for different mechanical properties (Figure 5d and Figure S5 for the PeaP). As before (Figure 4a), the stress-strain curve for the MeOH-treated film also shows a rapid increase in stress followed by the plateau region. However, the MeOH-treated film does not exhibit a three-stage pattern, and following the plateau region, a slow collapse of the mechanical properties at higher strain values is observed. In terms of the mechanical properties, the MeOH-treated SoyP film exhibits a lower tensile strength (~5 MPa), stemming from the different mechanical profiles described above, and a slightly higher Young's modulus (~230 MPa), resulting from changes in the initial stretching process (Table S3). However, the most profound change in the extracted mechanical properties is the elongation of fracture, exhibiting a ~4-fold decrease after the MeOH treatment directly related to the new nature of the MeOH-treated film being much denser.

Biodegradation Studies

The last section of our study concerns one of the most important characterizations of bioplastics, which is their end-of-life aspects and their biodegradation profile. At this point, we note that not all bioplastics are biodegradable. Bioplastic biodegradability is closely linked to the bioderived material used for its production and processing – whether a crosslinker was used, its type, and the plasticizer type. Due to our unique processing methodology involving the self-assembly of proteins without using a crosslinker or adding a common plasticizer, we can hypothesize a rapid biodegradation process of the films.

Biodegradation in Soil

We followed the biodegradation of the films in soil (Figure 6a-b). We placed the films inside the soil (Figure 6a) to mimic landfill conditions and on the soil surface (Figure 6b) to simulate more 'real-life' conditions of plastic disposal (Figure S9 for the PeaP). When placed inside the soil, we observed a very fast biodegradation profile, where complete biodegradation was reached after only 4 days (Figure 6a). Interestingly, identical biodegradation profiles were found for the as-prepared film and the MeOH-treated film despite their highly different degradation profiles and water uptake. The soil surface environment is poorer in bacteria than the bacteria-rich environment within the soil (as in compost). Nonetheless, we also observed a relatively fast biodegradation on the soil surface, where the films underwent complete biodegradation after 35 days (Fig-

ure 6b). As before, there was no difference between the as-prepared and the MeOH-treated films.

Biodegradation in an Aqueous Environment

Another major environmental problem of plastics use is their end-of-life features when reaching water sources (rivers, lakes, seas, and oceans). Plastics can frequently degrade into micro-plastics, which are not biodegraded and pose a danger to many life forms.[60,61] Likewise, though much faster, our new bioplastic also forms a dispersion upon water uptake and film collapse (as discussed above). Accordingly, our second biodegradation assay was performed within an aqueous environment containing bacteria. While the biodegradation evaluation within the soil was based on the common visual evaluation, here, we followed the amount of CO_2 produced by the bacteria. The measurement was conducted in closed vessels containing the SoyP/PeaP films as the only carbon source and compared to a cellulose powder (not film) as a common positive control, alongside a negative blank (see Figure 6c for the system schematic). Assessing CO_2 levels under aerobic conditions is the standardized test for determining the extent of a material's biodegradability.[62–64]

Considering the maximum theoretical CO_2 that can be produced from the carbon source calculated using the material's carbon content and weight, we transformed the accumulated CO_2 release (Figure S10) into a biodegradation percentage (Figure 6d). Usually, such biodegradation measurements include a lag time accounting for the adjustment period of the bacteria inside the inoculum to the new carbon source, followed by a slow or rapid rise in biodegradation rate until saturation (altogether, it can take a few months for the film to biodegrade). As seen in Figure 6d, the SoyP and PeaP films' biodegradation is very fast (much faster than the positive control), with no lag phase, and saturation commencing at ~70% after 28 days. The fast biodegradation of our films is directly related to their processing and morphology, i.e., non-crosslinked stacked layers of proteins in their native-like structural configuration. Proteins are excellent nutrients for all living things; hence, our films can provide nutrition for bacteria within the soil or in an aqueous environment.

Concluding Remarks

We present a simple, water-based, one-pot, energy-efficient formulation to produce biodegradable films/bioplastics. We use available plant-based proteins, namely SoyP and PeaP, without any purification steps, crosslinkers, or conventional plasticizers' addition. We used SoyP and PeaP here due to their sustainability and affordability. This is also the reason why these proteins are one of the most used for bioplastic formation. Nonetheless, the use of food-grade proteins for bioplastic formation is debatable as it competes with the use of the exact proteins for food applications. Nonetheless, the simple methodology introduced here can be easily adapted for a myriad of other proteins, and nowadays, we are working toward its
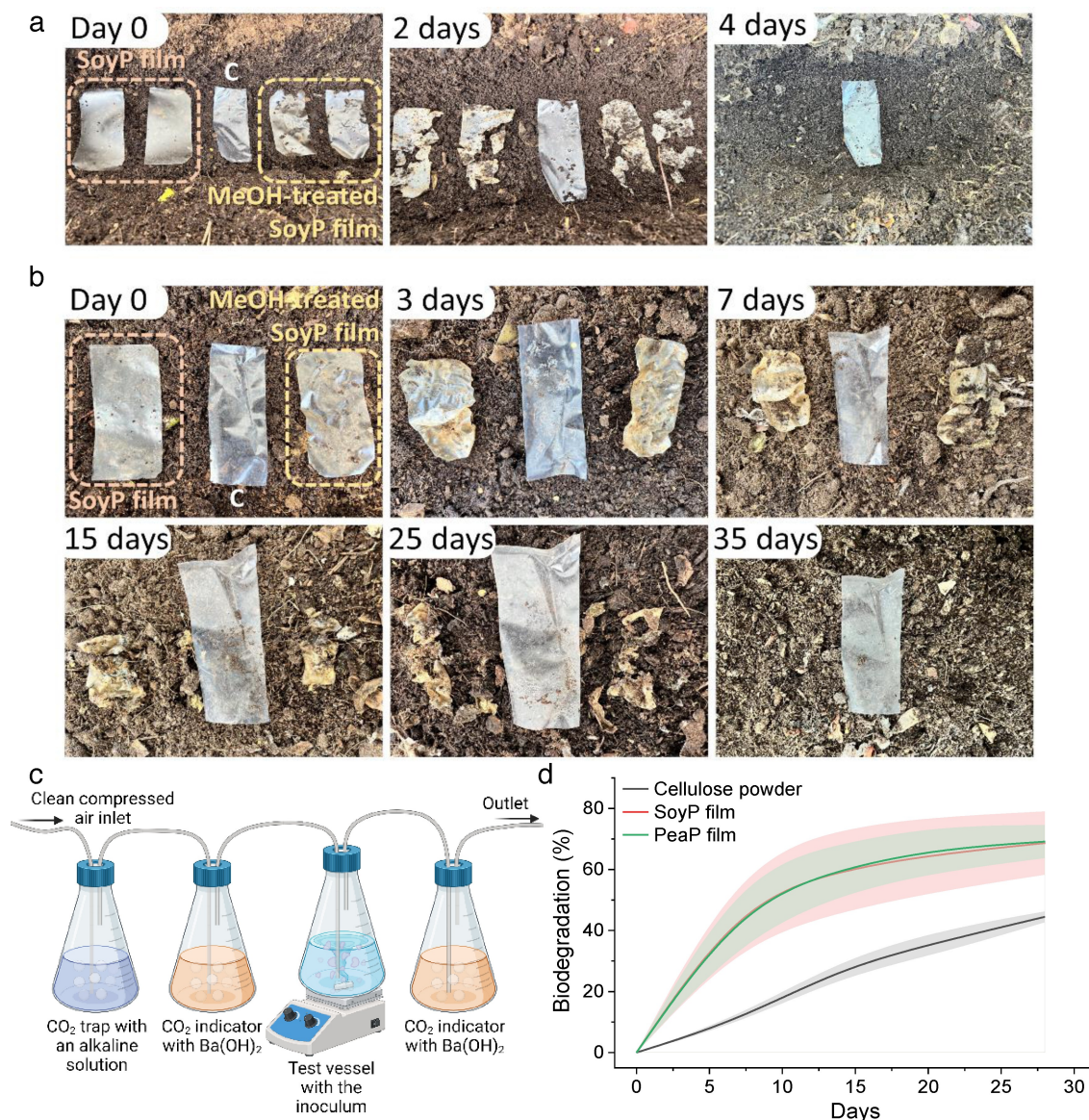
ChemSusChem

Research Article
doi.org/10.1002/cssc.202401567

Chemistry Europe
European Chemical
Societies Publishing

Figure 6. Biodegradation studies. a, and b, Images of the SoyP and MeOH-treated SoyP films during biodegradation within the soil (panel a) and on the soil surface (panel b) compared to a control (marked with C) sample (LDPE plastic). c, A schematic overview of the assay for biodegradation in an aqueous environment via CO_2 capture. d, The calculated biodegradation percentage of the SoyP and PeaP films in an aqueous environment. The shaded area represents the standard deviation of N = 3 samples.

adaptation to proteins that can be derived from primary or secondary waste sources in a closed-loop configuration, thus not 'competing' with the food industry.

The new process introduced here for using plant-derived proteins to produce free-standing transparent films is most likely the only one following all the relevant principles among the 12 principles of green chemistry. *Prevention* – our process produces no waste and, furthermore, it uses proteins from waste sources as the bioplastic main carbon source, thus preventing their waste; *Atom economy* – all materials used in the process (the protein and GlyA) are incorporated into the final product, as only water is being evaporated; *Less hazardous chemical syntheses/Designing safer chemicals* – although our process does not involve chemical synthesis or products, it is

design-oriented for safety and nonhazardousness; *Safer solvents and auxiliaries/Inherently safer chemistry for accident prevention* – only water (the greenest and safest possible solvent) is used as solvent, and no auxiliaries are being used; *Design for energy efficiency* – the only energy consuming part is the slight heating to 50 °C, which can be considered highly efficient compared to common processing of bioplastics or thermoplastics; *Use of renewable feedstocks* – the proteins used are considered sustainable from raw biomass, i.e., they do not deplete; *Reduce derivatives* – there is no derivatization in our process; *Design for degradation* – as discussed, our new bioplastics are designed for both degradation and biodegradation.

Our new films' uniqueness lies in the counterintuitive yet very simple processing technique that renders the straightfor-

ChemSusChem

Research Article
doi.org/10.1002/cssc.202401567

Chemistry
Europe
European Chemical
Societies Publishing

ward scalability of the process for industrial applications. In the described process, nonsoluble protein agglomerates undergo self-assembly via hydrogen bonding aided by the small GlyA molecules, resulting in an ordered and semicrystalline bioplastic upon water evaporation. We further show that during the self-assembly process, the protein changes its structure. Since the film formation is driven by hydrogen bonding between stacks of protein layers, the films are self-healable. It also leads to large amounts of water absorption when placed in an aqueous solution, resulting in their degradation, i.e., dispersion back to the agglomerated phase before film formation. We demonstrate that this property can be tuned by simply dipping the film in a MeOH solution, making it denser and thus less susceptible to water uptake and degradation. Nevertheless, the film's water solubility can be easily used for its recyclability; simply casting the dissolved solution of the film will result in its reformation upon water evaporation. Due to the film's production method, the final bioplastics can undergo rapid biodegradation on days' timescales in various conditions: inside the soil, i.e., in compost or landfill conditions, on the surface of the soil, and within an aqueous environment, as measured by CO_2 levels emitted during biodegradation.

Our new bioplastic also changes the perception of plastic recycling and upcycling. The current perception is that plastic recycling lowers the carbon footprint of its production from fossil-fuel-derived petrochemicals and its harmful impact on our planet. However, plastic recycling is a costly business involving its collection, sorting, and transportation to relevant factories for remaking new plastic products. We use plant-derived proteins that can be considered a sustainable source of raw biomass since they are mostly derived from sidsources; hence, their use helps lower the carbon footprint. For end-of-life aspects, we state that the disposal of our final bioplastic films has a benign environmental effect, in stark contrast to the detrimental impact of customary plastic disposal. This is because proteins are considered one of the best nutrition sources for all types of organisms, which also facilitates the rapid biodegradation of our new bioplastics. Hence, while recycling can be easily achieved for our new generation of plant-based bioplastics, it is not necessarily required. Nevertheless, to ensure a 'true circular economy', the upcycling and reusability of plastic is highly desirable, especially if the upcycling is performed by minimizing the consumption of raw material and maximizing the atom economy and energy efficiency of the process,[65] as presented here. The timescales of production and upcycling are also of prime importance,[24] and the minutes-to-hour time scales of both the production and recycling of our bioplastics represent a major advantage in polymer design for sustainability.

Methods

Materials for Film Formation

Soy protein (SoyP) from MP Biomedicals, pea protein (PeaP) from Pisane-Cosucra, and glycolic acid (GlyA) from Glentham Life Sciences were procured. SoyP and PeaP were extracted from defatted soy flakes and defatted yellow pea, respectively (Tables S1 and S2 for full details of the starting protein material). All experiments were performed using Milli-Q water.

Syntheses of the Protein Films

To make the protein film, 7 wt% of the protein powder (either SoyP or PeaP) was dispersed in water at 50°C and stirred for 30 minutes to form an aqueous suspension. GlyA (from a stock solution of 1.75 wt% GlyA in water) was mixed into the protein suspension at 50°C with a final GlyA concentration of 0.25 0.2 wt%. When GlyA was added, the dispersion transformed into a milky-white appearance. Stirring was continued at 50°C for an additional 30 minutes. The milky-white protein dispersion was drop-cast onto a plastic-made petri dish and kept there until the water evaporated (depending on the volume used) until a transparent protein film was formed. For methanol treatment, the film was placed in methanol for 10 minutes.

FTIR Measurements

A Bruker Tensor 27 spectrometer with an attenuated total reflectance (ATR) accessory was used for FTIR spectroscopy. For each measurement, the atmospheric background contribution was subtracted from the original FTIR spectrum. The FTIR spectra were averaged using the conditions of 4 cm^{-1} resolution with more than 68 individual scans. The second derivative of each spectrum was processed using the built-in Bruker software available in the instrument and analyzed using OriginPro2023 by deconvoluting the peaks under the amide I region (1600–1700 cm^{-1}) and integrating them.

X-Ray Scattering Diffraction (XRD) Measurements

XRD was performed on a Rigaku (SmartLab) high-resolution diffraction system. The system was equipped with a Hypix 3000 detector and beam energy of 1.5406 Å (8.04 KeV). The tests were performed at a 2θ range of 5°–90° in continuous mode with a scan rate of 5 degrees/minute and scan steps of 0.01 degrees using the 1D mode of the detector.

Scanning Electron Microscopy (SEM) Imaging

A cryo-SEM sample was prepared by placing ~3 µL of either SoyP suspension or GlyA-treated SoyP suspension between two metallic carriers. This was followed by high-pressure freezing (HPF) vitrification using a Leica EM ICE system. Following thermal fixation, the specimen was fractured at cryogenic temperatures under vacuum (Leica EM ACE900). To enhance contrast, the system allowed the removal of some of the vitrified liquid by sublimation. Transportation of the cryo-specimen was performed with a cooled and evacuated shuttle.

Upon completion of the procedure, the specimen on the specimen table was subsequently transferred onto the cryo-stage of the SEM through an airlock. The SEM stage was precooled to $-150\,°C$ and maintained at a high vacuum to ensure a contamination-free surface during the observation. The process of sublimating volatiles to improve topographic specimen contrast was performed inside the SEM by raising the temperature to $-110\,°C$ for approximately 1 minute. High-resolution SEM imaging was performed on a Zeiss Ultra Plus FEG-SEM with an acceleration voltage of 1 keV, applying a low-dose imaging procedure. The utilization of low-voltage and low-dose imaging was found to be sufficient to keep neutral even uncoated, nonconductive specimens with minimal radiation damage to the specimen.

Mechanical Testing

Mechanical testing of the protein films was conducted with cut films with dimensions of $2.5×1×0.02$ (length×width×thickness [cm]). The testing apparatus used was TA1, Ametek Instruments, Lloyd materials, equipped with a 50 N load cell. The samples were securely clamped within the mechanical tester and stressed at a constant speed of 2 mm/min until failure. All experiments were performed in triplicate to validate the overall shape of the stress ($σ$)–strain ($ε$) curves.

Water Stability Testing

To test the stability of the SoyP/PeaP film in pure water, films with dimensions of $4×4×0.02$ (length×width×thickness [cm]) were submerged in a 50 mL beaker containing 45 mL of water. The hydrated films were collected at predetermined time intervals, and the weight of the hydrated films was recorded.

Biodegradability Testing

Films with dimensions of $5×3×0.02$ (length×width×thickness [cm]) were placed either on the surface of an agricultural soil or 3 cm deep inside the soil. A commercial plastic control (LDPE plastic) was served as the control. The appearance of films was recorded digitally with time to check their biodegradation ability. An ISO 14852 protocol was used to study the biodegradation of the protein films within water with an inoculum. This study was carried out under aerobic conditions by measuring the % of biodegradability by the amount of evolved CO_2.[66]

Conflict of Interests

A patent application was submitted concerning the methodology introduced here.

Data Availability Statement

The data that support the findings of this study are available from the corresponding author upon reasonable request.

[1] J.-G. Rosenboom, R. Langer, G. Traverso, *Nat. Rev. Mater.* **2022**, *7*, 117–137.
[2] P. Stegmann, V. Daioglou, M. Londo, D. P. van Vuuren, M. Junginger, *Nature* **2022**, *612*, 272–276.
[3] R. Geyer, J. R. Jambeck, K. L. Law, *Sci. Adv.* **2017**, *3*, e1700782.
[4] G. Hayes, M. Laurel, D. MacKinnon, T. Zhao, H. A. Houck, C. R. Becer, *Chem. Rev.* **2023**, *123*, 2609–2734.
[5] P. Anastas, N. Eghbali, *Chem. Soc. Rev.* **2010**, *39*, 301–312.
[6] R. Mülhaupt, *Macromol. Chem. Phys.* **2013**, *214*, 159–174.
[7] D. K. Schneiderman, M. A. Hillmyer, *Macromolecules* **2017**, *50*, 3733–3749.
[8] Z. Wang, M. S. Ganewatta, C. Tang, *Prog. Polym. Sci.* **2020**, *101*, 101197.
[9] J. Su, K. Zhao, Y. Ren, L. Zhao, B. Wei, B. Liu, Y. Zhang, F. Wang, J. Li, Y. Liu, K. Liu, H. Zhang, *Angew. Chem. Int. Ed.* **2022**, *61*, e202117538.
[10] F. De Marchis, T. Vanzolini, E. Maricchiolo, M. Bellucci, M. Menotta, T. Di Mambro, A. Aluigi, A. Zattoni, A. Roda, V. Marassi, R. Crinelli, A. Pompa, *Biotechnol. J.* **2024**, *19*, 2300363.
[11] M. Häußler, M. Eck, D. Rothauer, S. Mecking, *Nature* **2021**, *590*, 423–427.
[12] A. Bazin, A. Duval, L. Avérous, E. Pollet, *Macromolecules* **2022**, *55*, 4256–4267.
[13] E. Ansink, L. Wijk, F. Zuidmeer, *Ecol. Econ.* **2022**, *191*, 107245.
[14] C. G. Otoni, H. M. C. Azeredo, B. D. Mattos, M. Beaumont, D. S. Correa, O. J. Rojas, *Adv. Mater.* **2021**, *33*, 2102520.
[15] V. V. T. Padil, C. Senan, S. Wacławek, M. Černík, S. Agarwal, R. S. Varma, *ACS Sustain. Chem. Eng.* **2019**, *7*, 5900–5911.
[16] Q. Xia, C. Chen, Y. Yao, J. Li, S. He, Y. Zhou, T. Li, X. Pan, Y. Yao, L. Hu, *Nat. Sustain.* **2021**, *4*, 627–635.
[17] A. Jones, A. Mandal, S. Sharma, *J. Appl. Polym. Sci.* **2015**, *132*, 41931.
[18] M. Pommet, A. Redl, M.-H. Morel, S. Domenek, S. Guilbert, *Macromol. Symp.* **2003**, *197*, 207–218.
[19] A. Miserez, J. Yu, P. Mohammadi, *Chem. Rev.* **2023**, *123*, 2049–2111.
[20] N. C. Abascal, L. Regan, *Open Biol.* **2018**, *8*, 180113.
[21] R. Nandi, Y. Agam, N. Amdursky, *Adv. Mater.* **2021**, *33*, 2101208.
[22] Y. Shen, A. Levin, A. Kamada, Z. Toprakcioglu, M. Rodriguez-Garcia, Y. Xu, T. P. J. Knowles, *ACS Nano* **2021**, *15*, 5819–5837.
[23] M. Peydayesh, M. Bagnani, R. Mezzenga, *ACS Sustain. Chem. Eng.* **2021**, *9*, 11916–11926.
[24] E. Y. X. Chen, *Nat. Sustain.* **2023**, *6*, 1140–1141.
[25] M. Jiménez-Rosado, J. F. Rubio-Valle, V. Perez-Puyana, A. Guerrero, A. Romero, *J. Appl. Polym. Sci.* **2021**, *138*, 50412.
[26] C. L. Murrieta-Martínez, H. Soto-Valdez, R. Pacheco-Aguilar, W. Torres-Arreola, F. Rodríguez-Felix, E. Márquez Ríos, *Packag. Technol. Sci.* **2018**, *31*, 113–122.
[27] F. Song, D.-L. Tang, X.-L. Wang, Y.-Z. Wang, *Biomacromolecules* **2011**, *12*, 3369–3380.
[28] N. Reddy, Y. Yang, *J. Appl. Polym. Sci.* **2013**, *130*, 729–738.
[29] A. Kamada, M. Rodriguez-Garcia, F. S. Ruggeri, Y. Shen, A. Levin, T. P. J. Knowles, *Nat. Commun.* **2021**, *12*, 3529.
[30] M. Yamada, S. Morimitsu, E. Hosono, T. Yamada, *Int. J. Biol. Macromol.* **2020**, *149*, 1077–1083.

ChemSusChem

Research Article
doi.org/10.1002/cssc.202401567

Chemistry Europe
European Chemical
Societies Publishing

[31] I. Paetau, C.-Z. Chen, J. Jane, *Ind. Eng. Chem. Res.* **1994**, *33*, 1821–1827.

[32] V. Perez-Puyana, P. Cuartero, M. Jiménez-Rosado, I. Martínez, A. Romero, *Food Packag. Shelf Life* **2022**, *32*, 100836.

[33] V. Perez-Puyana, M. Felix, A. Romero, A. Guerrero, *J. Sci. Food Agric.* **2017**, *97*, 2671–2674.

[34] X. Xu, L. Jiang, Z. Zhou, X. Wu, Y. Wang, *ACS Appl. Mater. Interf.* **2012**, *4*, 4331–4337.

[35] W.-Y. Xie, F. Song, X.-L. Wang, Y.-Z. Wang, *ACS Sustain. Chem. Eng.* **2017**, *5*, 869–875.

[36] Y. Han, M. Yu, L. Wang, *Ind. Crops Prod.* **2018**, *117*, 252–259.

[37] S. K. Park, D. H. Bae, K. C. Rhee, *J. Am. Oil Chemists' Soc.* **2000**, *77*, 879–884.

[38] Z. Wang, H. Kang, W. Zhang, S. Zhang, J. Li, *Polymers (Basel)* **2017**, *9*, 95.

[39] H. Kang, X. Song, Z. Wang, W. Zhang, S. Zhang, J. Li, *ACS Sustain. Chem. Eng.* **2016**, *4*, 4354–4360.

[40] C. Xia, L. Wang, Y. Dong, S. Zhang, S. Q. Shi, L. Cai, J. Li, *RSC Adv.* **2015**, *5*, 82765–82771.

[41] C. Sui, W. Zhang, F. Ye, X. Liu, G. Yu, *J. Appl. Polym. Sci.* **2016**, *133*, 43382.

[42] S. Zhang, C. Xia, Y. Dong, Y. Yan, J. Li, S. Q. Shi, L. Cai, *Ind. Crops Prod.* **2016**, *80*, 207–213.

[43] Q. Ye, Y. Han, J. Zhang, W. Zhang, C. Xia, J. Li, *J. Cleaner Prod.* **2019**, *214*, 125–131.

[44] X. Zhou, M. Zha, J. Cao, H. Yan, X. Feng, D. Chen, C. Yang, *ACS Sustain. Chem. Eng.* **2021**, *9*, 10948–10962.

[45] C. Lachaux, C. J. R. Frazao, F. Krauβer, N. Morin, T. Walther, J. M. François, *Front. Bioeng. Biotechnol.* **2019**, *7*, 359.

[46] P. K. Samantaray, A. Little, D. M. Haddleton, T. McNally, B. Tan, Z. Sun, W. Huang, Y. Ji, C. Wan, *Green Chem.* **2020**, *22*, 4055–4081.

[47] R. Tao, J. Sedman, A. Ismail, *Food Hydrocol.* **2022**, *122*, 107091.

[48] P. Chen, H. Tian, L. Zhang, P. R. Chang, *Ind. Eng. Chem. Res.* **2008**, *47*, 9389–9395.

[49] H. Yang, S. Yang, J. Kong, A. Dong, S. Yu, *Nat. Protoc.* **2015**, *10*, 382–396.

[50] D. J. Belton, R. Plowright, D. L. Kaplan, C. C. Perry, *Acta Biomater.* **2018**, *73*, 355–364.

[51] N. Aggarwal, D. Eliaz, H. Cohen, I. Rosenhek-Goldian, S. R. Cohen, A. Kozell, T. O. Mason, U. Shimanovich, *Commun. Chem.* **2021**, *4*, 62.

[52] F. Li, Q. Ye, Q. Gao, H. Chen, S. Q. Shi, W. Zhou, X. Li, C. Xia, J. Li, *ACS Appl. Mater. Interf.* **2019**, *11*, 16107–16116.

[53] Y. Wei, S. Jiang, X. Li, J. Li, Y. Dong, S. Q. Shi, J. Li, Z. Fang, *ACS Appl. Mater. Interf.* **2021**, *13*, 37617–37627.

[54] J. Li, S. Jiang, Y. Wei, X. Li, S. Q. Shi, W. Zhang, J. Li, *Compos. B* **2021**, *211*, 108645.

[55] K. Li, S. Jin, X. Li, S. Q. Shi, J. Li, *J. Cleaner Prod.* **2021**, *285*, 125504.

[56] Z. Xie, B.-L. Hu, R.-W. Li, Q. Zhang, *ACS Omega* **2021**, *6*, 9319–9333.

[57] D. L. Taylor, *Adv. Mater.* **2016**, *28*, 9060–9093.

[58] L. Cera, G. M. Gonzalez, Q. Liu, S. Choi, C. O. Chantre, J. Lee, R. Gabardi, M. C. Choi, K. Shin, K. K. Parker, *Nat. Mater.* **2021**, *20*, 242–249.

[59] S. Hwang, Q. Shao, H. Williams, C. Hilty, Y. Q. Gao, *J. Phys. Chem. B* **2011**, *115*, 6653–6660.

[60] J. Woodward, J. Li, J. Rothwell, R. Hurley, *Nat. Sustain.* **2021**, *4*, 793–802.

[61] N. Gontard, G. David, A. Guilbert, J. Sohn, *Nat. Sustain.* **2022**, *5*, 472–478.

[62] M. S. Kim, H. Chang, L. Zheng, Q. Yan, B. F. Pfleger, J. Klier, K. Nelson, E. L. W. Majumder, G. W. Huber, *Chem. Rev.* **2023**, *123*, 9915–9939.

[63] O. García-Depraect, R. Lebrero, S. Rodriguez-Vega, S. Bordel, F. Santos-Beneit, L. J. Martínez-Mendoza, R. Aragão Börner, T. Börner, R. Muñoz, *Bioresour. Technol.* **2022**, *344*, 126265.

[64] J.-F. Su, X.-Y. Yuan, Z. Huang, W.-L. Xia, *Polym. Degrad. Stab.* **2010**, *95*, 1226–1237.

[65] D. Ma, *Nat. Sustain.* **2023**, *6*, 1142–1143.

[66] ISO 14852:2021, in https://www.iso.org/standard/80303.html, Vol. ISO/TC 61/SC 14 Environmental aspects, ISO **2021**, 19.